Local carboplatin delivery and tissue distribution in livers after radiofrequency ablation

A. Szymanski-Exner,[1] A. Gallacher,[2] N. T. Stowe,[3] B. Weinberg,[1] J. R. Haaga,[4] J. Gao[1,4]
[1]*Department of Biomedical Engineering, Case Western Reserve University, 10900 Euclid Avenue, Cleveland, Ohio*
[2]*Department of Analytical Chemistry, Ricerca, LLC, Concord, Ohio*
[3]*Department of Surgery, Case Western Reserve University School of Medicine, Cleveland, Ohio*
[4]*Department of Radiology, University Hospitals of Cleveland, Cleveland, Ohio*

Received 9 December 2002; accepted 20 December 2002

Abstract: This study investigated the local drug pharmacokinetics of intralesional drug delivery after radiofrequency ablation of the liver. We hypothesized that the tissue architecture damaged by the ablation process facilitates the drug penetration in the liver and potentially enlarges the therapeutic margin in the local treatment of cancer. The delivery rate and tissue distribution of carboplatin, an anticancer agent, released from poly(D,L-lactide-co-glycolide) implants into rat livers after radiofrequency ablation were quantified by atomic absorption spectroscopy. Results showed that carboplatin clearance through blood perfusion was significantly slower in the ablated livers, leading to a more extensive tissue retention and distribution of the drug. The concentration of Pt at the implant–tissue interface ranged from 234 to 1440 μg Pt/(g liver) in the ablated livers over 144 h versus 56 to 177 μg Pt/(g liver) in the normal tissue. The maximum penetration distance at which Pt level reached above 6 μg/g (calculated based on a reported IC_{90} value for carboplatin) was 8–10 mm and 4–6 mm in ablated and normal liver, respectively. Histological analysis of the necrotic lesions showed widespread destruction of tissue structure and vasculature, supporting the initial hypothesis. This study demonstrated that intralesional drug delivery could provide a sustained, elevated concentration of anticancer drug at the ablation boundary that has the potential to eliminate residual cancer cells surviving radiofrequency ablation. © 2003 Wiley Periodicals, Inc. J Biomed Mater Res 67A: 510-516, 2003

Key words: drug delivery; tissue distribution; atomic absorption spectroscopy; pharmacokinetics; radiofrequency ablation

INTRODUCTION

Image-guided radiofrequency (RF) ablation has been successfully used in recent years as a minimally invasive therapy to treat unresectable liver tumors.[1–8] In this procedure, imaging methods such as X-ray computed tomography, magnetic resonance imaging, or ultrasound guides the percutaneous insertion of a needle electrode to the site of a tumor. Electric current at radio frequency is applied through the needle, leading to ionic agitation, increased temperature, and finally coagulative necrosis.[2–6] The procedure is simple, quick, and can be performed on an outpatient basis.[3,4] Studies have shown that although RF ablation is able to destroy majority of the tumor tissue, tumor recurrence has been reported in many cases because of the incomplete elimination of all the cancer cells.[3,6,7] To address this limitation, other minimally invasive interventional procedures, such as intralesional drug therapy, are being explored.

Currently, research efforts in our group focus on the development of a combination therapy consisting of RF ablation and local chemotherapy for the treatment of solid tumors. The therapy includes the following steps: first, a small drug-loaded cylindrical implant, the polymer millirod, will be fabricated using established methods.[9] This device is composed of an active agent entrapped in a biodegradable poly(lactic-*co*-glycolic acid) (PLGA) matrix. Second, under image guidance, a tumor will be treated with RF ablation followed by implantation of millirod(s) directly into tumor tissues to provide site-specific delivery of the selected agent. The active agent will be released from the polymer matrix directly into tumor tissue at a controlled rate over time to eliminate the residual cancer cells.

Local drug delivery is a powerful technique that has the potential to become a mainstream alternative to

Correspondence to: J. Gao; e-mail: jmg23@po.cwru.edu
Contract grant sponsor: National Institutes of Health; contract grant number: R21 CA93993

conventional systemic chemotherapy. This mode of drug administration can deliver the drug to a site of action at a significantly higher concentration than is possible with intravenous injection or oral delivery. It can also maintain the concentration within the therapeutic window to avoid unnecessary toxicity. Particularly, local delivery is beneficial for drugs (especially anticancer drugs) with narrow therapeutic indices or short *in vivo* half-lives to maximize their therapeutic efficacy.

For a local drug therapy to attain maximum efficacy, it must deliver the therapeutic dose of a drug to the target area without substantially affecting the normal tissues. Frequently, the drug released from the implant must travel a significant distance and reach the site of action in its active state, and its ability to do so will depend highly on the properties of the drug as well as on the property of the tissue. Other groups have examined the effects of cell density on drug distribution in tissue and have determined that a decreased cell density due to apoptosis enhances tissue penetration.[10–12] Currently, data on local drug release and tissue pharmacokinetics are limited but need to be quantified for the successful development of a local drug delivery system. This is true especially in complex tissue environments, such as thermally ablated tissue. Because the viable and ablated tissue structure varies drastically, with the ablated region lacking viable cells and vasculature, we predict that this difference will significantly affect the local drug pharmacokinetics in tissues.

In this study, we examined the release kinetics and tissue distribution of carboplatin as it was released from the polymer millirod in ablated liver tissues. The drug distribution profiles provide information on the local drug pharmacokinetics in ablated tissues and were correlated with tissue structure from histology analysis. Results from this study provide the fundamental understanding of structure-property relationships between *in vivo* drug transport properties and liver structures, which is essential for the future design of sustained release formulations in conjunction with RF ablation for the treatment of liver tumors.

MATERIALS AND METHODS

Materials

PLGA (lactide:glycolide = 1:1, 0.65 dL/g inherent viscosity) was purchased from Birmingham Polymers, Inc. (Birmingham, AL). Carboplatin (cis-diammine(1,1-cyclobutanedicarboxylato) platinum) and poly(vinyl alcohol) (13–23 kDa) was purchased from Sigma-Aldrich (Milwaukee, WI). D(+)-Glucose was purchased from Fluka (Milwaukee, WI). Phosphate-buffered saline (PBS), sodium hydroxide (NaOH, 0.2*M*), nitric acid (70%, trace metal grade), and methylene chloride were obtained from Fisher Scientific (Pittsburgh, PA). Single-element platinum standard (NIST traceable) was purchased from CPI International (Santa Rosa, CA). Teflon tubes were purchased from McMaster–Carr Supply Company (Cleveland, OH). Sprague–Dawley rats were obtained from Charles River Laboratories (Wilmington, MA).

Polymer implant fabrication and *in vitro* characterization

Millirod implants were fabricated according to a previously established compression-heat molding procedure.[9] Briefly, PLGA microspheres (approx. 4 μm diameter) were mixed with carboplatin to form a uniform mixture, and D(+)-glucose was added to the mixtures in order to expedite the rate of release. The homogeneously mixed powder was placed in a mold and compressed at 4.6×10^6 Pa at 90°C for 2 h. The resulting cylindrical millirods have an average diameter of 1.62 mm and a theoretical loading density of 10% carboplatin with 35% glucose (w/w).

The *in vitro* release of carboplatin from the millirods was measured in PBS (pH 7.4). Typically, segments of millirods (approx. 8 mm in length) were submerged in 10 mL of PBS and placed in an orbital shaker (New Brunswick Scientific, model C24) at 37°C and 100 rpm agitation. At each sampling point, the millirod was removed from the vial and placed into 10 mL of fresh PBS. The retained sample was analyzed using flameless, graphite-furnace atomic absorption spectroscopy (GF-AAS, PerkinElmer model 4100ZL). This method has been a widely accepted method of examining levels of various metals in tissue and body fluids.[13–15] The method is a spectrophotometric technique based on the absorption of radiant energy by atoms.[16] First, five single-element platinum standards (NIST traceable) were prepared in deionized water at concentrations of 10, 25, 50, 100, and 500 μg Pt/L to establish the calibration curve. The linear correlation coefficients for all the curves (area counts for Pt at 265.9 nm vs. concentration) were greater than 0.999 before analysis. The platinum concentration in the retained sample (Pt, μg/mL) was determined by quantitative serial dilution (250×) in water followed by their interpolative assay against the standard curve. The platinum content was then converted to reflect the total carboplatin release based on the weight percentage of Pt to the drug molecule. The average amount of carboplatin remaining in the implants was calculated from this data and was standardized to the initial measured length of each implant. The total concentration of carboplatin was calculated based on measurements of the drug in completely degraded implants.

RF ablation and millirod implantation in rat livers

Animal procedures followed an approved protocol by the Institutional Animal Care and Use Committee. Male Sprague–Dawley rats (250–350 g) were anesthetized using an intraperitoneal injection of sodium pentobarbital (4 mg/100 g). The abdomen was swabbed with betadine solution, and

mercaine (bupivacaine, 0.1 mL) was injected subcutaneously at the incision site prior to the start of surgery. The liver was exposed through an incision in the midsection. In the animals undergoing ablation, the liver capsule of the medial lobe was first perforated with an 18-gauge hypodermic needle, and the liver tissue was ablated with a 19-gauge needle electrode (Radionics®, Burlington, MA 01803) at 90 ± 3°C for 2 min. The ablation procedure followed a previously established method.[8,17] After ablation, millirods (5–7 mm in length) were implanted into the needle electrode track. Millirods of the same composition used in the ablated lobes were implanted into nonablated livers for comparison. After implantation, a small piece of cotton was sutured on top of the implantation site to seal the wound and prevent the implant from slipping out. The animals received Buprenex (buprenorphine, 0.05–0.1 mg/kg) after the surgery and were allowed to recover. The animals were then euthanized with Fatal Plus (concentrated sodium pentobarbital), and livers were removed and stored at −80°C. Animals were divided into six experimental groups with endpoints of 1, 6, 24, 48, 96, and 144 h. Each group consisted of six rats with implants in normal livers ($n = 3$) and ablated livers ($n = 3$).

Sample preparation and analysis with atomic absorption spectroscopy

The platinum content in livers and explanted millirods was also analyzed with atomic absorption spectroscopy (AAS). In preparation for AAS analysis, the livers were divided into three segments around the center (implantation site) and three 2-mm thick slices were sectioned from each segment. These were cut into 2-mm wide strips and the six strips closest to the implant (radial distance of 12 mm) were retained for analysis. These samples were deposited into previously weighed, 4-mL glass scintillation vials. The vials were weighed again to determine the wet mass of each liver segment. Sample digestion was conducted using a novel dry-block procedure (compared to the standard microwave digestion). The 4-mL vials were placed into dry-block incubators and 100 μL of 70% nitric acid was added to each vial. The samples were heated to 70°C for 1 h and digestion was aided by addition of 50 μL hydrogen peroxide after 20, 30, and 50 min. The clear sample solutions were transferred to 15-mL Falcon centrifuge tubes that were diluted to 5 mL with distilled water and stored at 4°C until analysis. To determine carboplatin release in vivo, the explanted millirods were degraded in 2 mL of 0.2M NaOH at 37°C for 1 week. The solution was neutralized with addition of 2 mL of 0.2M nitric acid and filtered with 0.45-μm syringe filters before AAS analysis. The platinum concentrations in the above solutions were determined by interpolative assay against the standard curve (10–500 μg Pt/L) as described in the previous section. The μg/L measurements were converted to μg/(g liver) by multiplication of the sample volume and division by the original wet tissue weight. The explant measurements were converted to mg/cm as the remaining quantity of carboplatin per unit length of the millirod.

The $t_{1/2}$ was calculated based on exponential decay curve fit to the average release data. The tissue penetration distance was calculated as the maximum distance at which the Pt concentration reaches above 6 μg/g, a value calculated based on the IC_{90} (10 μg/mL)[18] carboplatin concentration to the VX-2 cancer cells. The area under the concentration-time curve (AUC) for carboplatin in ablated liver tissue over 144 h was calculated using the trapezoid rule for the implant/tissue interface and ablation boundary. An unpaired, two-tailed Student t test with a 95% confidence interval was used to determined significant differences among data sets. Significant outliers were discarded on basis of the Grubbs test ($\alpha = 0.05$).

Histological analysis

All liver samples underwent gross histological examination and microscopic analysis. The diameter of the visible ablated area perpendicular to the ablation needle tract was measured three times and an average measurement of the ablation area was calculated. Representative sections of the specimens were removed and fixed in 10% formalin solution. The preserved sections were embedded in paraffin, sectioned into 5-μm slices and stained with hematoxylin and eosin. The hematoxylin and eosin sections were examined to determine the normal tissue structure surrounding the implanted millirod and the damage inflicted by the implantation trauma and thermal ablation.

RESULTS

In vitro release of carboplatin in PBS buffer

Figure 1 shows the average release profile of carboplatin in PBS buffer (pH 7.4) at 37°C. The data are represented as carboplatin remaining in the millirod over time and is standardized by the length of each implant (mg/cm). The cumulative release follows the Higuchi model ($C_{drug} = kt^n$, $n = 0.5 \pm 0.03$) with a value of $t_{1/2}$ at 42 ± 8 h. In addition, 2.0 ± 0.2 and 3.8 ± 0.3 mg carboplatin/cm were released after 24 and 96 h, respectively ($n = 4$). The reproducibility of the fabrication procedure is demonstrated by a reasonably low standard deviation (<0.3 mg/cm, $n = 4$) at all time points.

In vivo release of carboplatin in rat livers

The *in vivo* release of carboplatin in ablated and normal rat livers is shown in Figure 1. Compared with the *in vitro* release, the standard deviation in *in vivo* release data is significantly greater, particularly at earlier time points ($t \leq 24$ h). Although carboplatin release appears to be faster in ablated livers than normal livers in the first day after implantation, it should be

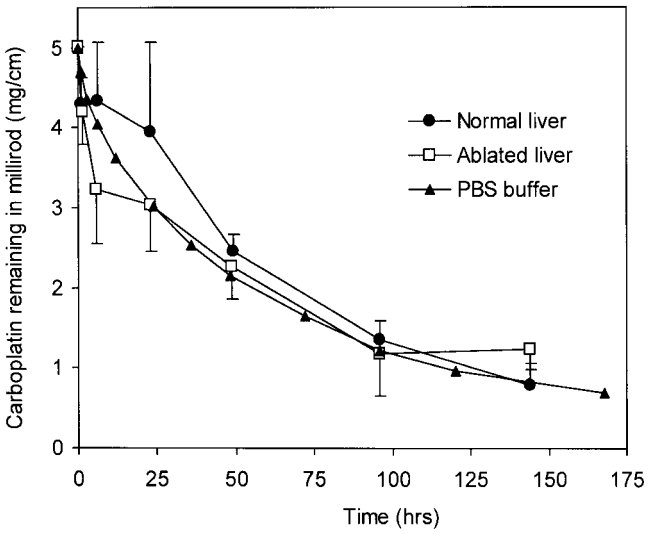

Figure 1. Release of carboplatin from millirod implants *in vitro* ($n = 4$) and *in vivo* ($n = 3$) in ablated (□) and normal (●) liver. Dara are shown as weight of carboplatin remaining in millirod and standardized based on the length of individual implants. Portions of error bars (reflecting standard deviation measurements) were omitted for clarity. In the *in vitro* release (▲), the standard deviation was below 0.3 mg/cm at all time points.

noted the difference is not statistically significant (e.g. the p value from the Student t test is 0.13 and 0.28 at 6 and 24 h, respectively). Release half-life was determined as 51 ± 10 and 44 ± 15 h for normal and ablated tissue, respectively. When examining the raw data, we observed a comparable release amount of carboplatin at longer time points in both systems, with 3.7 ± 0.2 and 3.8 ± 0.5 mg carboplatin/cm released after 96 h in normal and ablated livers, respectively. This data demonstrates similar overall release kinetics in the two liver environments as well as in PBS buffer (3.8 ± 0.3 mg/cm at 96 h).

Distribution of carboplatin in normal and ablated liver tissues

Figure 2(A,B) shows the tissue distribution of carboplatin in platinum concentrations as a function of distance in ablated ($n = 9$) and normal ($n = 9$) liver tissues. Data show significantly more carboplatin were retained in the ablated tissue over the normal tissue. In the livers treated with RF ablation [Fig. 2(A)], the range of platinum in the tissue exceeds 1400 μg Pt/(g liver) at the millirod/tissue interface, and the concentration rises steadily through 48 h and decreases thereafter. In contrast, the range of Pt in the normal liver [Fig. 2(B)] consistently remains below 200 μg Pt/(g liver), and the concentration varies randomly throughout the 6 days after implantation. The maximum tissue penetration distance, at which the Pt concentration reaches above 6 μg/g liver, was found to be between 8–10 mm in the ablated liver at 1 and 96 h. During the other time points, the maximum distance was between 4–6 mm. In the normal liver, the maximum penetration distance was found to be between 0–2 mm at all but one time point and between 4–6 mm in the first hour.

The change in carboplatin concentration over time at the implant/tissue interface and the distal ablation boundary is shown in Figure 2(C,D). At implant/tissue interface, carboplatin in the ablated livers reaches $1.4 \pm 0.6 \times 10^3$ μg/g liver (C_{max}, $n = 9$) at 48 h and is 24 times higher than that in the normal liver [61 ± 45 μg/g, Fig. 2(C)]. At the approximate ablation boundary (4–6 mm), the carboplatin concentration was at least two times higher in the ablated liver at all time points, and 14 times higher at 144 h [Fig. 2(D)]. Although the differences in measured Pt are consistent, it should be noted that some measurements (especially the Pt content in normal tissue) at this distance are below the detection limit of the atomic absorption technique, and may not be accurate.

The AUC at the implant/tissue interface was calculated to be 234.6 and 28.5 (mg/g)*h for carboplatin in ablated and normal liver, respectively. The AUC at the ablation boundary (or 4–6 mm from the implant) was calculated to be 4.8 (mg/g)*h in ablated and 0.8 (mg/g)*h in normal liver. All AUC values are reported in mg carboplatin (not Pt) for clinical relevance.

Histological analysis

The gross morphology of the tissue surrounding the millirod was significantly altered in the ablated liver site. The ablation radius ranged from 3.8 to 5.8 mm (average radius = 4.8 ± 0.9 mm). Millirod implantation in the ablated lesion resulted in little or no additional injury to the tissue as observed by the easy removal of the millirod from the implantation site. Upon gross examination, the tissue at the millirod boundary appeared to be identical to that further away from the implantation site in the ablated area. In comparison, the implantation site in normal liver showed a slight morphological change in the surrounding tissue. The tissue adjacent to the implant appeared white and granular, and the implant was difficult to remove, possibly indicating an early response of the tissue to injury.

Microscopic examination of the implantation site showed a vastly different tissue structure in the ablated liver tissue with notable changes over 6 days [Fig. 3(A,D)]. The tissue structure near the implantation site showed the same architecture as in the rest of the ablated area [Fig. 3(A,B)]. The cellular structure was different from normal liver cells and corresponds

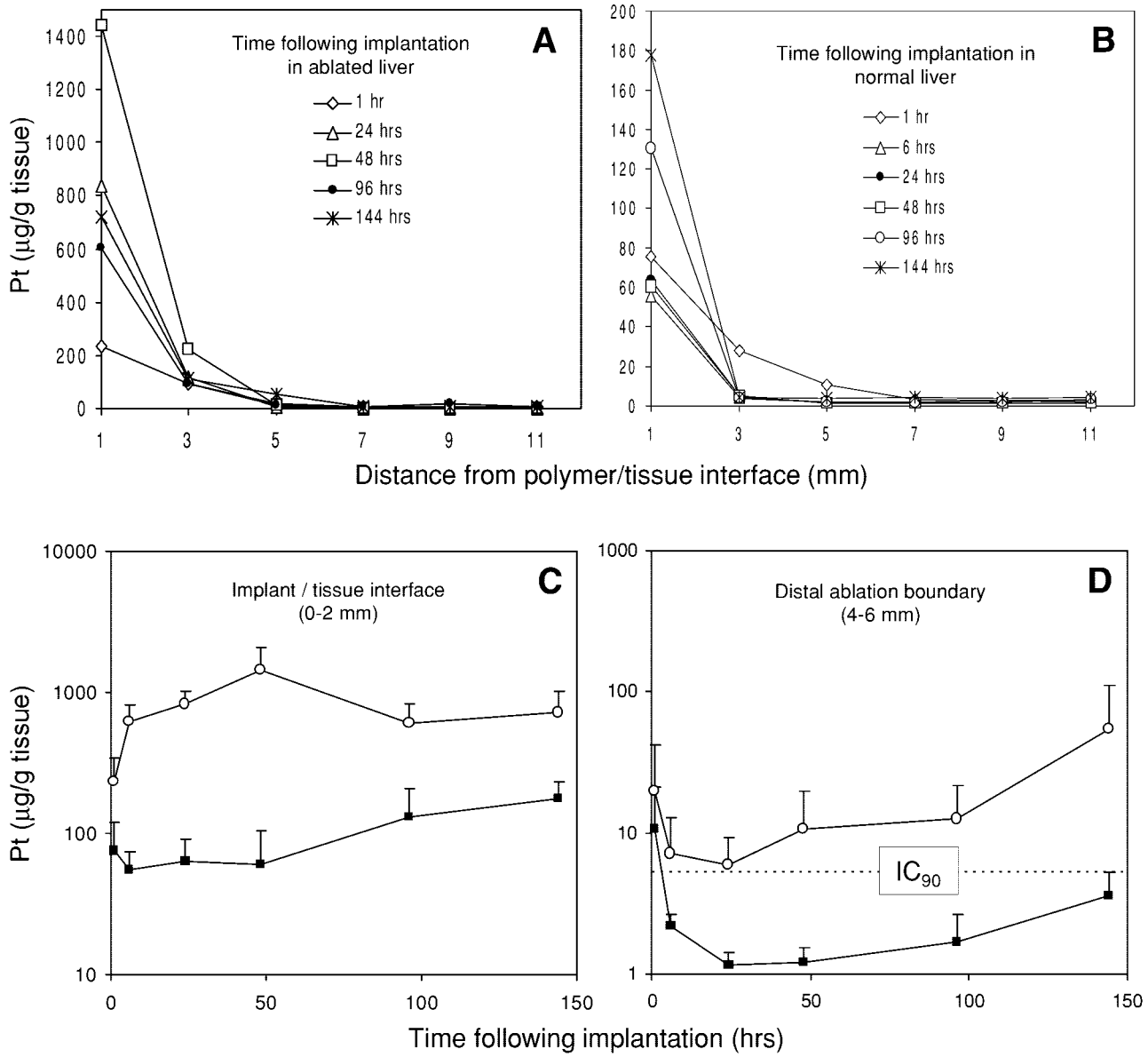

Figure 2. Local drug pharmacokinetics of carboplatin in normal and ablated liver over 144 h. (A) Tissue distribution in ablated liver. Carboplatin distribution increases initially and reaches a maximum at 48 h. The distribution data at 6 h superimpose with the 96-h data and were omitted. (B) Tissue distribution in normal liver, where no obvious time-dependent trend was observed. Error bars were omitted for clarity in (A) and (B). (C) Pt concentration at the implant/tissue interface in normal (■) and ablated (○) livers. (D) Pt concentration at the distal ablation boundary in ablated livers. Pt concentration at the same distance in normal liver is shown for comparison. Dashed line represents the IC_{90} value of carboplatin to VX-2 cancer cells from the literature. Error bars reflect standard error ($n = 9$).

to features of coagulative necrosis with picnotic nuclei and disrupted and irregular cytoplasm. The sinusoidal structure was destroyed and the interstitial space was increased. At the distal edge of the ablated area, and at the interface of the ablated and normal liver tissue, a ring of inflammatory infiltrate, composed of lymphocytes and monocytes, was observed. This ring is more apparent at later time points starting at 24 h and increasing through 144 h. The cell nuclei in the necrotic area become increasingly sparse as the necrosis spreads, and fibroblasts and granulation tissue are visible at the distal ablation boundary at 96 and 144 h [Fig. 3(C,D)].

DISCUSSION

The therapeutic efficacy of the intralesional drug delivery system addressed in this study is highly dependent on the local drug pharmacokinetics in the tissue environment surrounding the implantation site. Characterization of the *in vivo* drug release kinetics and drug penetration in ablated tissue is critical in providing the necessary experimental data for the development of these delivery systems.

The *in vitro* release kinetics of carboplatin in PBS buffer ($t_{1/2} = 42 \pm 8$ h) agrees reasonably well with

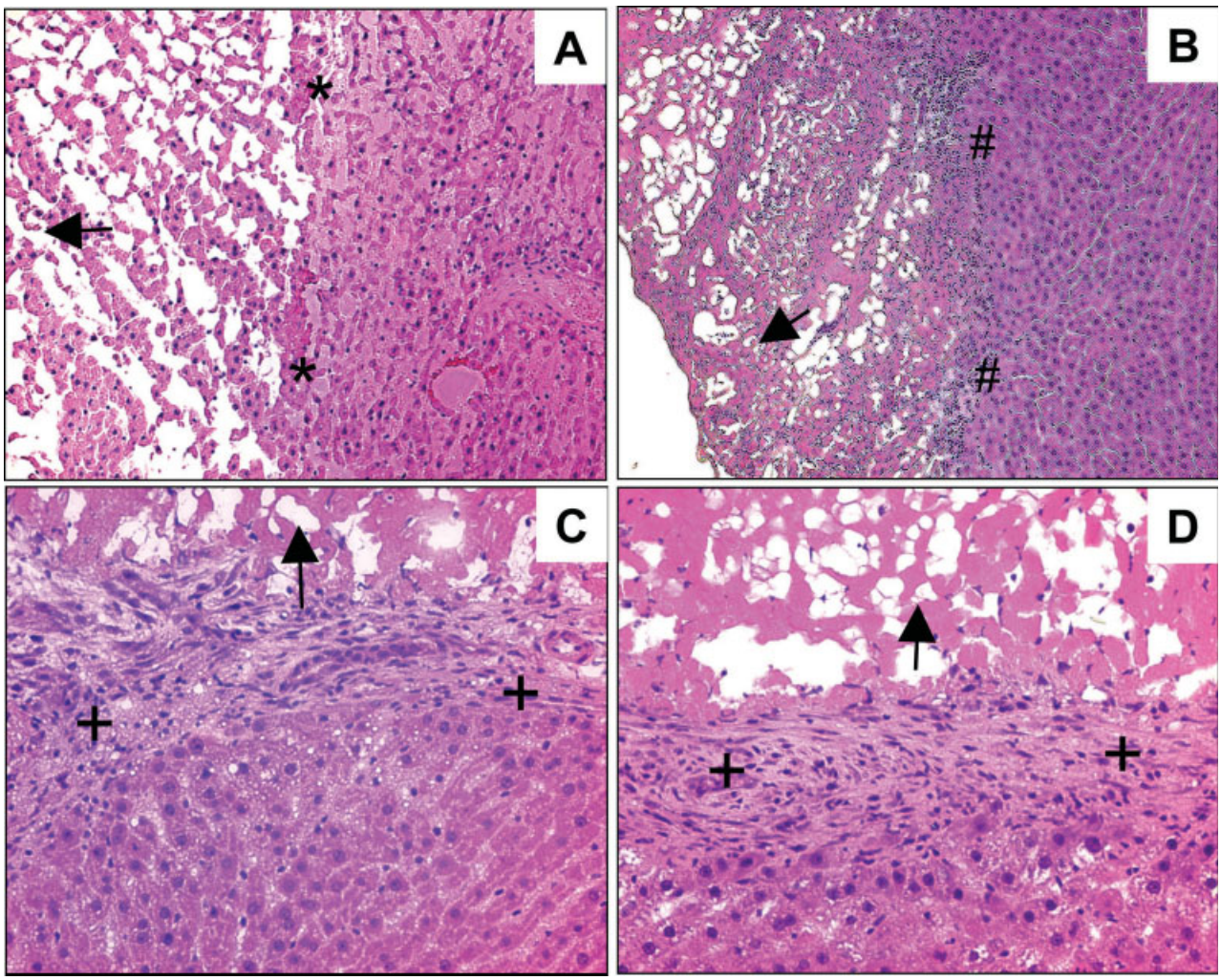

Figure 3. Histological changes in liver tissue after RF ablation . Arrows indicated the location of ablated tissue and implant position. (A) After 24 h, the boundary between normal and ablated tissue is clearly defined (*). (B) At 48 h, the ring of inflammatory cells is clearly visible (#). (C) At 96 h, the inflammatory response gives way to fibroblasts and collagen formation (+). (D) At 144 h, the disorganized structure of the fibrous capsule is clearly visible (+). The original magnification was 100× for (A) and (B) and 200× for (C) and (D). [Color figure can be viewed in the online issue, which is available at www.interscience.wiley.com.]

those in normal liver ($t_{1/2}$ = 51 ± 10 h) and ablated liver ($t_{1/2}$ = 44 ± 15 h) *in vivo*. The *in vivo* release kinetics showed larger experimental variability, which may reflect the heterogeneous liver environments in different animals. Results from current study indicate slightly faster release of carboplatin from polymer millirods in ablated liver than normal liver; however, this difference is not statistically significant. In comparison, the retention, distribution and penetration of carboplatin are significantly different in the two tissue environments. Carboplatin retention is approximately one order of magnitude higher in the ablated liver over normal liver [Fig. 2(A,B)]. In addition, drug penetration is significantly greater in ablated liver with a maximum penetration distance of 8–10 mm compared to mostly 2 mm in the normal liver.

The different pharmacokinetics of carboplatin in ablated and normal liver can be correlated to structural changes in the liver following RF ablation. The histology analysis documented these changes in the ablated lesion over 6 days. During this time it is possible to observe morphological changes in hepatocytes undergoing coagulative necrosis, where the cells shrink and nuclei become increasingly sparse as they are cleared out from the injured area. These results are in agreement with those reported previously by our group[17] as well as others.[5,8] More importantly, the histological analysis of ablated lesions confirms the severe destruction of organized sinusoidal capillary structure and other liver vasculature visible in normal tissue (not shown). The lack of carboplatin clearance through blood perfusion in ablated tissue is a determinant factor for the greater retention and penetration of carboplatin. Without drug loss from perfusion, drug dif-

fusion becomes the dominant process of transport in ablated liver, and leads to significantly higher penetration distance over normal liver. Wound healing response to the heat-induced injury may also affect the local drug pharmacokinetics. At the ablation boundary, a ring of inflammatory cells is observed from 24 to 96 h [Fig. 3(B,C)], and fibroblasts are observed forming a fibrous capsule around the ablated area after 96 h [Fig. 3(D)]. The formation of fibrous capsule may cause the elevated platinum concentration at the ablation boundary at 144 h [Fig. 2(D)] over the other time points.

In our proposed combination therapy, intralesional drug delivery aims to eliminate the residual cancer cells surviving RF ablation. Therefore, the ablation boundary is the targeted site of action and the concentration-time relationships at this location are important for an effective carboplatin therapy. Our study showed that carboplatin reached its therapeutic concentration (IC_{90} of carboplatin to VX-2 cancer cells) at the ablation boundary for all the time points over 144 h [Fig. 2(D)]. The AUC value at the ablation boundary was determined to be 4.8 (mg/g)*h in ablated liver, six times more than normal liver [0.8 (mg/g)*h] at the same distance. Since clinical AUC values are normally calculated from the plasma drug concentrations, the tissue measurements from this study cannot be compared with the clinical data. Nonetheless, as regional and local drug delivery becomes a more accepted therapy, these measurements may become essential in describing the local tissue pharmacokinetics and evaluating the effectiveness of drug delivery systems.

CONCLUSIONS

The data obtained in this study successfully support our hypothesis that radiofrequency ablation of tissue increases the maximum penetration distance of a drug and allows the drug to be consistently elevated above therapeutic concentration at the site of action. The tissue penetration was three times higher in the ablated tissue and drug concentration was found to be an order of magnitude higher at most distances from the tissue/implant interface as compared with similar implants in normal livers. The mode of action for this striking difference is the destruction of vasculature and loss of perfusion resulting from the ablation process, which is supported by gross and microscopic examination of the histology sections. Although this study demonstrates that the drug can reach the ablation boundary, further studies on a tumor model are necessary to evaluate the increased efficacy of the combination therapy (RF ablation + local drug delivery) over RF ablation alone. These studies are currently being conducted in our group with the rabbit VX-2 tumor model.

The authors thank Dr. James Anderson for his help with the histology analysis.

References

1. Becker GJ. 2000 RSNA annual oration in diagnostic radiology: The future of interventional radiology. Radiology 2001;220: 281–292.
2. Lewin JS, Connell CF, Duerk JL, Chung YC, Clampitt ME, Spisak J, Gazelle GS, Haaga JR. Interactive MRI-guided radiofrequency interstitial thermal ablation of abdominal tumors: clinical trial for evaluation of safety and feasibility. J Magn Reson Imaging 1998;8:40–47.
3. Dodd GD III, Soulen MC, Kane RA, Livraghi T, Lees WR, Yamashita Y, Gillams AR, Karahan OI, Rhim H. Minimally invasive treatment of malignant hepatic tumors: at the threshold of a major breakthrough. Radiographics 2000;20:9–27.
4. Rhim H, Dodd GD III. Radiofrequency thermal ablation of liver tumors. J Clin Ultrasound 1999; 27:221–229.
5. Goldberg SN, Gazelle GS, Compton CC, Mueller PR, Tanabe KK. Treatment of intrahepatic malignancy with radiofrequency ablation: radiologic-pathologic correlation. Cancer 2000;88:2452–2463.
6. Goldberg SN, Gazelle GS. Radiofrequency tissue ablation: physical principles and techniques for increasing coagulation necrosis. Hepatogastroenterology 2001;48:359–367.
7. Bartolozzi C, Crocetti L, Cioni D, Donati FM, Lencioni R. Assessment of therapeutic effect of liver tumor ablation procedures. Hepatogastroenterology 2001;48:352–358.
8. Boaz TL, Lewin JS, Chung YC, Duerk JL, Clampitt ME, Haaga JR. MR monitoring of MR-guided radiofrequency thermal ablation of normal liver in an animal model. J Magn Reson Imaging 1998;8:64–69.
9. Qian F, Szymanski A, Gao J. Fabrication and Characterization of Controlled Release Poly(D,L-Lactide-co-Glycolide) Millirods. J Biomed Mater Res 2001;55:512–522.
10. Au JLS, Jang SH, Wientjes MG. Clinical aspects of drug delivery to tumors. J Control Release 2002;78:81–95.
11. Kuh HJ, Jang SH, Wientjes MG, Weaver JR, Au JLS. Determinants of Paclitaxel Penetration and Accumulation in Human Solid Tumor. J Positron Emission Tomogr 1999;290:871–880.
12. Jang SH, Wientjes MG, Au JLS. Enhancement of paclitaxel delivery to solid tumors by apoptosis-inducing pretreatment: effect of treatment schedule. J Positron Emission Tomogr 2001; 296:1035–1042.
13. Duffull SB, Robinson BA. Clinical pharmacokinetics and dose optimisation of carboplatin. Clin Pharmacokinet 1997;33:161–83.
14. Milacic R, Cemazar M, Sersa G. Determination of platinum in tumour tissues after cisplatin therapy by electrothermal atomic absorption spectrometry. J Pharm Biomed Anal 1997;16:343–348.
15. Meerum Terwogt JM, Tibben MM, Welbank H, Schellens JH, Beijnen JH. Validated method for the determination of platinum from a liposomal source (SPI-77) in human plasma using graphite furnace Zeeman atomic absorption spectrometry. Fresenius J Anal Chem 2000;366:298–302.
16. Shugar GJ. Atomic Absorption Spectroscopy. In: Shugar R, Bauman L, Shugar-Bauman R, editors. Chemical technicians' ready reference handbook, 3rd ed. New York: McGraw-Hill, Inc.; 1990. p 751–763.
17. Szymanski-Exner A, Stowe NT, Lazebnik RS, Salem KA, Wilson DL, Haaga JR, Gao J. Noninvasive monitoring of local drug release in a rabbit radiofrequency (RF) ablation model using x-ray computed tomography. J Control Release 2002;83:415–425.
18. Pauser S, Wagner S, Lippmann M, Pohlen U, Reszka R, Wolf KJ. Evaluation of efficient chemoembolization mixtures by magnetic resonance imaging therapy monitoring: An experimental study on the VX2 tumor in the rabbit liver. Cancer Res 1996;56:1863–1867.